Journal of the Brazilian Society of Mechanical Sciences and Engineering (2019) 41:89
https://doi.org/10.1007/s40430-019-1587-0

TECHNICAL PAPER

Parameter optimisation to combine low energy consumption with high surface integrity in turning Mg/Al_2O_3 hybrid composites under dry and MQL conditions

E. Suneesh[1] · **M. Sivapragash**[2]

Received: 11 November 2018 / Accepted: 14 January 2019 / Published online: 22 January 2019

Abstract
A high strength-to-mass ratio makes the use of metal matrix composites acceptable for a wide range of engineering applications. However, their use is often complicated, and machining such composites involves several challenges. During the machining process, controllable machining parameters need to be optimised to achieve multiple objectives. In this work, an attempt was made to streamline the turning parameters of a magnesium/alumina hybrid composite under dry and minimum quantity lubrication (MQL) cutting conditions. Experiments were carried out based on Taguchi's L18 orthogonal array. The input parameters (i.e. cutting conditions, cutting speed, feed and depth of the cut) were considered the cutting factors, while surface roughness, cutting force, specific power consumption, and cutting temperature were the response variables. A grey relational analysis (GRA) and the techniques for order preferences by similarity to ideal solution (TOPSIS) method were employed to improve the straight turning process of hybrid composites and to optimise the input control factors. The percentage contribution of each input parameter was identified by creating an analysis of variance (ANOVA) table. Based on the data given in the response table and the ANOVA table for the GRA and TOPSIS, feed rate was found to be the most influential parameter of those investigated in the present study, followed by the depth of cut, cutting conditions, and cutting speed. The GRA and TOPSIS produced two unique sets of optimised parameters. The optimised parameter combinations obtained using the GRA method were cutting condition = MQL, cutting speed = 100 m/min, feed rate = 0.15 mm/rev, and depth of cut = 0.50 mm; using the TOPSIS, the optimal value for cutting speed changed to 150 m/min when all other parameter values were kept the same as they were for the GRA. However, from the results of the validation tests, it was clear that the optimised parameters obtained from the TOPSIS produced a machined composite with better properties than the composite produced using the GRA.

Keywords Turning · Magnesium hybrid composite · Quality characteristics · Taguchi method · Grey relational analysis · TOPSIS

1 Introduction

Presently, the demand for light-weight materials to be used in automotive and aerospace applications is increasing because of the need for weight reduction and improved fuel economy [1, 2]. Though aluminium (Al) and magnesium (Mg) have both gained the interest of researchers, Mg has the lowest density among all conventionally used metals and, thus, has become the candidate with the most potential to meet the above-described demand [3]. Though cast and wrought Mg alloys are widely used, they are less desirable than other materials concerning certain properties, such as corrosion resistance and high- temperature creep strength [4, 5]. Currently, Mg metal matrix composites (MMCs)

Technical Editor: Lincoln Cardoso Brandão.

✉ E. Suneesh
suneeshe555@gmail.com

[1] Department of Production Engineering, Vidya Academy of Science & Technology, Thalakottukara, Thrissur, Kerala 680510, India

[2] Department of Mechanical Engineering, PSN College of Engineering & Technology, Tirunelveli, India

with improved mechanical properties are being developed for advanced applications [6, 7]. The influence of different reinforcements (single type) and processing methods on Mg-based MMCs have been studied, and it has been found that ceramic reinforcements, such as alumina (Al_2O_3) and silicon carbide (SiC) can provide excellent high-temperature properties as well as unique mechanical properties [8–10]. Mg-based MMCs containing micro-ceramic reinforcements were succeeded by Mg nanocomposites as a result of the latter's reduced ductility and the former's lower fracture toughness [11–18]. Although Mg nanocomposites display excellent ductility and weight-saving characteristics, nanoparticle clusters sometimes form and reduce the strength of these nanocomposites [18–20]. Mg hybrid composites are a class of Mg-based materials that have recently been considered for structural applications. Wong et al. [21] observed that the addition of micro- and nano-sized Al_2O_3 particles to pure Mg can bring about remarkable improvements in hardness, elastic modulus, 0.2% yield strength (YS), and ultimate tensile strength (UTS) while compromising ductility.

Mg-based composites can be processed through a variety of methods, such as powder metallurgy (PM), stir casting, squeeze casting, the disintegrated melt deposition technique, etc., and most of these processes yield near net shapes. Sometimes, though, just the right machining process needs to be adopted to achieve the desired shape, dimensions, and surface finish of these composites. Turning operation is one of the most commonly used metal cutting processes, as it is simple and economical. The general machining of pure Mg or of Mg alloys is considered relatively easy, as it requires relatively little force and power. However, machining Mg often involves the problem of chip ignition. At high cutting speeds, increased cutting zone temperatures cause chips to ignite, as the ignition temperature of Mg chips (430 °C) is well below its melting temperature (650 °C) [22, 23].

Another issue that arises during Mg machining is associated with the application of coolants. Coolants are usually applied during machining to reduce the temperature that is reached during the process. Water-based coolants cannot be used for the machining of Mg-based materials because Mg can react with water-based coolants to form hydrogen, which is explosive and flammable [23–25]. Further, even though Mg is a soft metal, the machining of Mg-based MMCs is difficult because it is challenging to drill tiny holes with high aspect ratios into Mg-based MMCs. This is because machining such composites often leads to sudden tool wear, tool breakage, and chip disposal from the miniaturised holes [26]. Though Mg MMCs exhibit desirable properties, the difficulties associated with their machining restrict their widespread use in various industries [27].

As the quality of products in manufacturing industries is assessed in terms of surface finish, recent research studies have focused on examining the effect of processing attributes on the surface characteristics of produced components. Mg-based hybrid MMCs are useful in advanced applications, such as those of the aerospace industry, where considerations of surface roughness are significant. This is because surface roughness affects the strength of parts during operation; hence, great care is taken to achieve optimum surface finish during the manufacturing process [28]. The functionality of machined parts greatly depends upon surface finish. In addition, an adequate surface finish assures improved corrosion resistance, tribological properties, surface appearance, and fatigue resistance, along with reduced manufacturing costs [29–31].

The effect of different cutting environments on the machining of UNS M11917 materials was investigated by Rubio et al. [25]. The results suggest that a low feed rate achieves the best surface finish irrespective of the cutting condition. In a similar study, the influence of cutting parameters on surface roughness and flank wear was examined by Turgay Kıvak [32]. The optimisation study was conducted using an L18 full-factorial design with a mixed orthogonal array (OA). The optimisation results indicate that feed rate had the greatest influence on surface roughness, while flank wear was largely affected by cutting speed. Similar studies were conducted by other researchers who found that cutting feed had the greatest influence on the surface characteristics of Mg-based materials [33–36]. In addition, optimisations were performed to minimise the cutting force and the energy consumption required during the machining process [37, 38].

Recently, dry machining has been replaced by the application of cutting fluids. Cutting fluids improve tool life and the surface finish of products, thereby increasing the performance and efficiency of the machining process [39]. A major drawback of the use of cutting fluids during Mg machining is that it causes environmental and health hazards (as mentioned earlier).

To accommodate the benefits of cutting fluids and to make production environment-friendly, researchers have focused on reducing the use of cutting fluids and exploring advanced methods, like minimum quantity lubrication (MQL), the complete suppression of cutting fluids, etc. [40]. In MQL, the cutting zone between the tool and workpiece receives a small amount of liquid (~ 50 ml/h), which provides cooling while the pressurised air that reaches the cutting zone acts as a lubricant [41]. Thus, MQL utilises conventional cutting fluids to provide a clean and healthy production process. Machining using MQL offers several advantages over dry and wet machining, such as a low cutting temperature, high surface finish, and dimensional accuracy. These benefits have encouraged researchers to extensively study MQL-assisted machining; after several investigations, researchers have now adapted MQL-assisted machining to model certain quality characteristics,

such as surface finish, tool life, cutting force, cutting temperature, etc.

Limited studies have examined the machinability characteristics of Mg-based materials under MQL conditions. A few of these are summarised presently. In one investigation on the MQL-assisted turning of Mg alloys, Carou et al. [42] analysed the intermittent turning of UNS M11917 Mg at different machining conditions. A full-factorial experimental design and analysis of variance (ANOVA) were used for the statistical analysis. Feed rate was identified as the most significant factor for all the tests. In another study, Carou et al. [43] provided a detailed review of the application of the MQL system in turning operations for different materials. Similar studies were also conducted to study the influence of MQL on turning process outcomes, such as surface finish, cutting temperature, tool life, etc. [37, 44–46].

Multiple characteristic optimisation methods have recently become the focal point of research aiming to improve the quality of products (by increasing the surface finish) and minimise the cost (by reducing cutting force and energy consumption) of the machining process. Among the different optimisation techniques, the grey relational analysis (GRA) and technique for order preferences by similarity to ideal solution (TOPSIS) were widely used to solve complex multi-response problems [47, 48]. Both are simple and efficient techniques used to solve multi-criteria decision problems and, thus, have attracted researchers' interest. In both optimisation techniques, the multi-objective function is solved by converting it into a single-objective function. Buldum et al. [49] investigated a multi-response optimisation technique in the oblique turning of AZ91D Mg alloy aimed to achieve minimum cutting force and surface roughness and maximum material removal rate (MRR) using a Taguchi—GRA approach. Cutting depth was noted as the most significant factor that influenced multiple responses.

Gopal et al. [50] optimised the material and milling parameters to reduce cutting force, surface roughness, and temperature during the end milling of Mg MMCs. GRA and TOPSIS were used to accomplish the multi-objective optimisation, and both approaches provided similar optimum parameter conditions.

Four response variables are considered in the present study—surface roughness, cutting force, specific cutting energy (or specific power consumption), and cutting zone temperature. As already mentioned, surface roughness is a measure of aesthetic value, and it influences a machined product's performance regarding corrosion resistance, electrical conductivity, fatigue life, etc. [29–31]. Cutting force is associated with the deterioration of a tool and the consumption of power during cutting. Tool breakage, surface accuracy, tool wear, machine vibrations, and cutting temperature vary with an increase in cutting force [51].

The power required to remove a unit volume of material from the workpiece is known as specific power consumption. Specific power consumption has a high correlation with tool wear, cutting force, surface quality, and chip formation mechanism [52]. Surface roughness and cutting force decrease with a reduction in specific power consumption. A reduction in specific power consumption provides an efficient and economical manufacturing process, whereas MRR has no effect on process efficiency. Also, an evaluation of specific power consumption involves the estimation of MRR. Hence, in the present study, specific power consumption (or specific energy) is chosen over MRR as one of the objectives.

The temperature in metal cutting is another significant factor influencing the production rate, and it depends directly on the cutting parameters. A high cutting temperature during the machining process has detrimental effects on both the tool and the workpiece. The cutting tool suffers rapid wear, thermal flaking, and tends to form a build-up on its edge when the cutting temperature is high; meanwhile, the workpiece is subject to dimensional inaccuracy and surface damage [53]. Though most of the heat developed during cutting is eliminated from the cutting areas as the chips fly away, it is, nevertheless, essential to control the amount of heat that remains in the contact zone between the tool and the workpiece, as doing so minimises the amount of harm done to the tool and the workpiece.

A literature survey reveals that a certain quantum of work has been conducted to examine the influence of various process variables on different machining responses during the machining of Mg-based materials. Most of these works have focused on the turning, drilling, or milling of pure Mg or Mg alloys; Mg-based MMCs have received relatively little attention. Also, only a very few models have been constructed for which cutting condition (MQL vs. dry) was a variable. Hence, the present investigation has been carried out to fill this knowledge gap. An attempt is made presently to identify the optimum parameter combination for a better surface finish and reduced cutting force, specific power consumption, and temperature via GRA and TOPSIS. Micro- and nano-alumina-reinforced Mg-3.0Zn-0.7Zr-1.0Cu alloy hybrid composites produced via the PM process were used throughout the optimisation process. Taguchi's L18 mixed design OA was employed to derive the experimental procedure as discussed below.

2 Experimental procedure

2.1 Preparation of the hybrid composite

A quaternary Mg–Zn–Zr–Cu (Mg–3Zn–0.7Zr–1Cu) alloy was used as the base matrix in this study. High-purity Mg

Table 1 Composition of the base matrix

Designation	Zn (Wt.%)	Zr (Wt.%)	Cu (Wt.%)	Mg (Wt.%)
Mg-3Zn-0.7Zr-1Cu alloy	3	0.7	1	Remaining

Table 2 Composition of the prepared hybrid composites

Material/Designation	Base alloy (wt.%)	Al_2O_3 (wt.%)	
		Micro	Nano
Mg-3Zn-0.7Zr-1Cu/3 µ Al_2O_3 + 0.5 nano Al_2O_3	96.5	3	0.5

powder (size: 50–65 µm, purity: 97%), Zn powder (size: 45–75 µm, purity: 97.5%), Zr powder (size: 50 µm, purity: 99.5%), and Cu powder (size: 45–75 µm, purity: 99%) were used to prepare the matrix compositions. Micro-Al_2O_3 powder, coupled with nano-Al_2O_3 powder, was used as the hybrid reinforcements. Micro-Al_2O_3 with an average particle size of 20–50 µm and a purity of 99.9% was obtained from Alfa Aesar, USA. A planetary ball milling machine (Pulverisette-5, Fritsch, Germany) was used to prepare the nano-Al_2O_3 particles. The compositions of the matrix materials and the hybrid composites are described in Tables 1 and 2, respectively.

The composition of the matrix alloy was prepared before the addition of the reinforcement particles. The matrix alloy powder composition and hybrid Al_2O_3 reinforcements were first weighed carefully using an electronic balance (Shimadzu 2-kg capacity, 0.01 g accuracy) and then mixed to form a blend in a mechanical alloying machine (RETSCH PM-400) which was operated at a speed of 200 rpm for 1 h in order to obtain a perfect mix of the composite composition. During the blending process, the proportions of the micro-Al_2O_3 and nano-Al_2O_3 were fixed at 3% and 0.5 wt.%, respectively. The composite mixtures obtained after blending were allowed to dry and were then compacted in a uniaxial hydraulic press (WMW 150 T) at a pressure of 50–60 N/m^2 to form green compacts which measured 65 mm in diameter and 35 mm in length. These green compacts were then sintered at 400 °C at a heating rate of 5 °C/min using an electric muffle furnace (HASTHAS HSI-115, Max. temp. = 1100 °C) and were then allowed to cool gradually to room temperature while still in the furnace.

The sintered billets were subsequently hot extruded in a uniaxial hydraulic press at a temperature of 400 °C. Before hot extrusion, samples were coated with colloidal graphite to prevent the samples from sticking to the dye. Using an extrusion ratio of 25:1, rods that were 500–800 mm long and 12.5 mm in diameter were produced from the sintered billets. To relieve the stress developed in the samples during the compaction and hot extrusion processes, the extruded rods were further heated in a muffle furnace at 260 °C for 15 min. The composites were prepared to accommodate typical light-weight structure applications in the automotive industry in which weight reduction is considered extremely important. The sintered and extruded samples prepared in this study are shown in Fig. 1. The procedure and experimental set-up used for preparing the composites are given in extensive detail in another author's work [54]. The mechanical properties of the alloy are given in Table 3.

Table 3 Mechanical properties of the extruded Mg/Al_2O_3 hybrid composite

Tensile strength	232 MPa
Density	1.83 gm/cm^3
Hardness	102 HV
Young's modulus	59 GPa

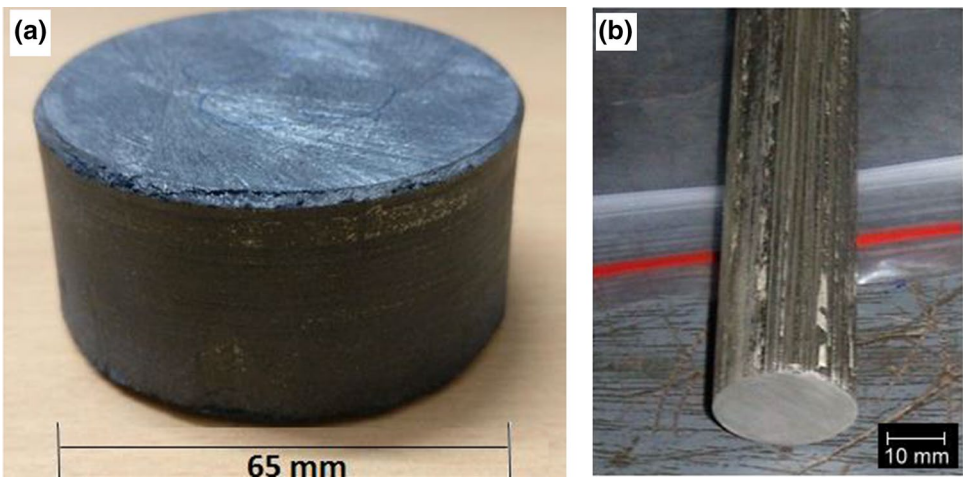

Fig. 1 Mg-3Zn-0.7Zr-1Cu + 3µ Al2O3 + 0.5 nano-Al_2O_3 hybrid composite: **a** compacted and sintered specimen and **b** extruded rod

2.2 Experimental set-up and measurement of output responses

The experiments were carried out on a Nagmati-175 all geared lathe. The workpiece rods used for machining under dry and MQL conditions were 12 mm diameter and 150 mm length. Cutting was done with uncoated tungsten carbide inserts which were clamped in a K12 tool holder. Straight cutting oil provided the MQL in this study. A nozzle with carrier air was used to apply the very fine lubricating jet to the cutting zone at a pressure of 6 bars and a flow rate of 40 ml/h.

Surface roughness (R_a), major cutting force (F), specific power consumption (P_{sp}) and cutting temperature (T) were considered as the performance measures. Surface roughness was determined using a TR240 surface roughness tester. The cutting force measurement was taken by a piezoelectric-type Kistler Dynamometer. An Amprobe IR750 infrared thermometer was used to record the temperatures reached during machining; the measurable range of the instrument is − 50 °C to 1500 °C. The specific power consumption can be calculated as follows [55]:

$$P_{sp} = \frac{F \times V}{\text{MRR}} \tag{1}$$

$$\text{MRR} = V.f.d \tag{2}$$

In the above equation, V is the cutting speed in m/min, F is the major cutting force in N, f is the feed in mm/rev, and d is the depth of the cut in mm.

The measurements were taken in line with the feed direction, and three repeated measurements were taken to arrive at average values. The interrelation between the processing variables and output responses is illustrated in Fig. 2. The experimental procedure is shown in Fig. 3.

2.3 Experimental factors and design of experiment (DoE)

Along with cutting condition (dry or MQL), cutting speed (V), feed rate (f), and depth of cut (d) are considered input parameters. Each of these parameters (with their respective levels) is illustrated in Table 4. The levels of each machining factor (speed, feed, and depth of cut) are assigned based on practical experience and the results of the pilot study conducted for this purpose.

In this study, four control factors are considered, one of which has two levels and three of which have three levels. The influence of these control factors on the performance measures (R_a, F, P_{sp}, and T) of the composites samples was examined using the Taguchi approach. The Taguchi method was chosen because it requires relatively few experimental runs to design an experimental plan. As the number of experiments is reduced, the Taguchi approach requires less time to complete tests, making it an economical option. Therefore, according to the degrees of freedom (DOF), study, and mixed level control factors, the L18 Taguchi OA is used for the present experimental study. Therefore, 18 trails are needed for the optimisation as shown in Table 5.

3 Methodology for optimising the hybrid composite turning process

The use of a signal-to-noise-ratio-based Taguchi method coupled with a GRA and TOPSIS is proposed in this study to optimise the process variables. The general optimisation procedure's scheme is depicted in Fig. 4.

3.1 S/N-ratio-based Taguchi optimisation

The Taguchi-based optimisation approach used in this study requires the individual measured responses to be converted into signal-to-noise (S/N) ratios. An S/N ratio is used to identify which control factors reduce the variability in a process by reducing the impacts of noise

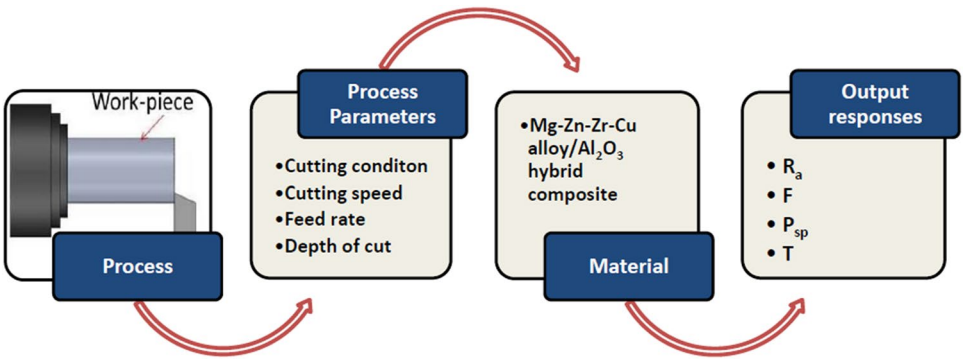

Fig. 2 Interrelations between the process variables and the output responses

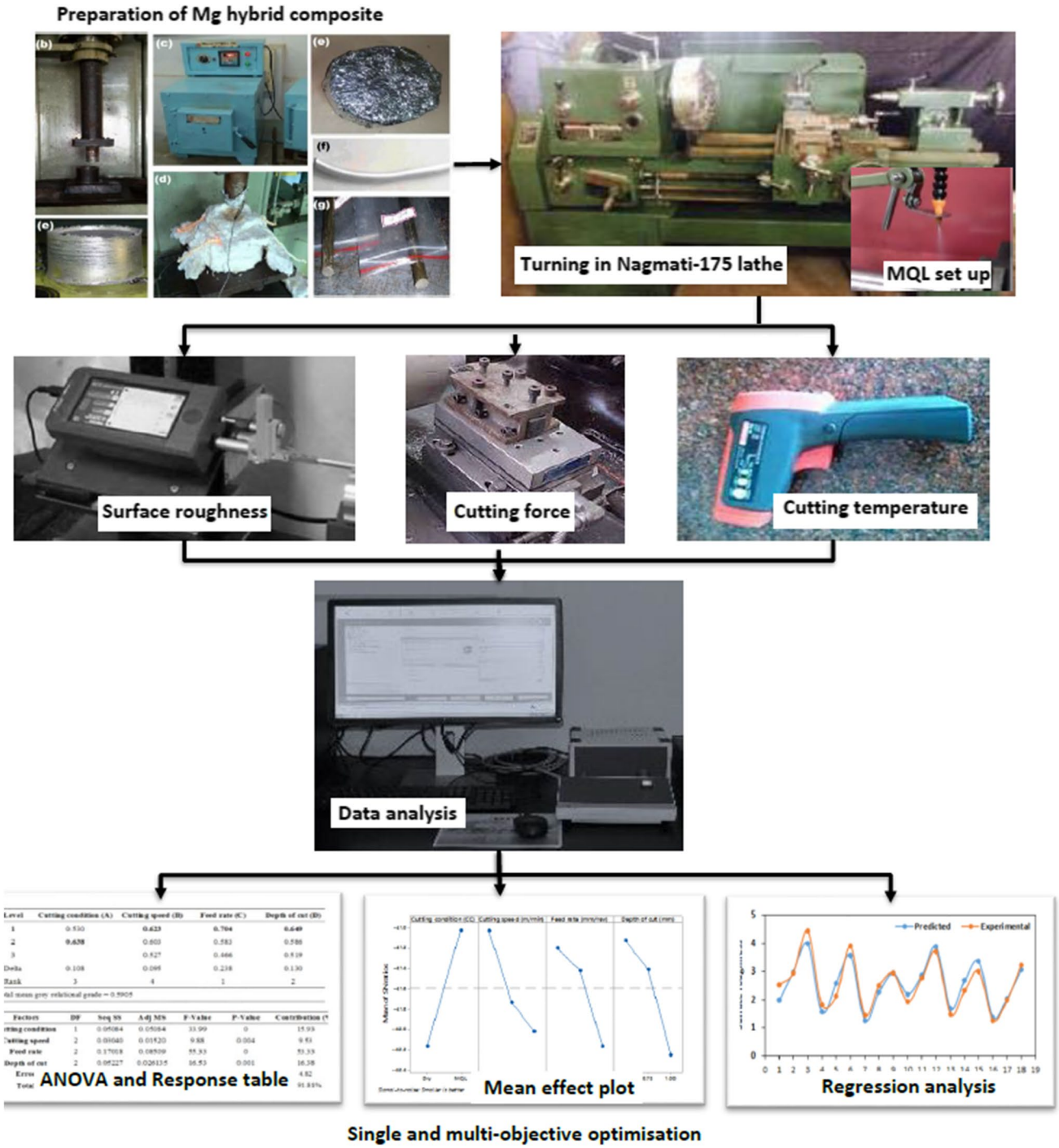

Fig. 3 Experimental procedure for the turning and optimisation of Mg/Al_2O_3 hybrid composites

Table 4 Turning process parameters and their levels

Code	Process parameters	Symbol	Unit	Levels		
				1	2	3
A	Cutting condition	CC	–	Dry	MQL	–
B	Cutting speed	*V*	m/min	100	150	200
C	Feed rate	*f*	mm/rev	0.15	0.30	0.45
D	Depth of cut	*d*	mm	0.50	0.75	1.00

Table 5 Experimental design based on L18 orthogonal array

Trial No.	Designation	Machining parameters			
		CC	V	f	d
1	A1B1C1D1	Dry	100	0.15	0.50
2	A1B1C2D2	Dry	100	0.30	0.75
3	A1B1C3D3	Dry	100	0.45	1.00
4	A1B2C1D1	Dry	150	0.15	0.50
5	A1B2C2D2	Dry	150	0.30	0.75
6	A1B2C3D3	Dry	150	0.45	1.00
7	A1B3C1D2	Dry	200	0.15	0.75
8	A1B3C2D3	Dry	200	0.30	1.00
9	A1B3C3D1	Dry	200	0.45	0.50
10	A2B1C1D3	MQL	100	0.15	1.00
11	A2B1C2D1	MQL	100	0.30	0.50
12	A2B1C3D2	MQL	100	0.45	0.75
13	A2B2C1D2	MQL	150	0.15	0.75
14	A2B2C2D3	MQL	150	0.30	1.00
15	A2B2C3D1	MQL	150	0.45	0.50
16	A2B3C1D3	MQL	200	0.15	1.00
17	A2B3C2D1	MQL	200	0.30	0.50
18	A2B3D3C2	MQL	200	0.45	0.75

factors (uncontrollable factors). The term "signal" denotes the positive effect for an output characteristic, while the term "noise" refers to an undesirable effect for the output characteristic. An S/N ratio evaluates the deviation of performance characteristics from the desired value, and a high value of an S/N ratio indicates an optimum level of control factors. S/N ratios are determined using three types of quality characteristics: smaller-the-better, nominal-the-better, and larger-the-better. The objective of the present work is to optimise turning process parameters to minimise R_a, F, P_{sp} and T. Since the values of these performance characteristics need to be as low as possible, the smaller-the-better criterion is selected for these parameters.

The following equation can be used to estimate the S/N ratio value with the smaller-the-better criteria [56]:

$$S/N = -10 \log \left(\frac{1}{n} \sum_{i=1}^{n} y_i^2 \right) \tag{3}$$

In this equation, i is the experiment number, y_i is the experimental result of the ith experiment, and n is the total number of experiments.

For the whole investigation range, the S/N ratios were calculated using Eq. (3) for R_a, F, P_{sp} and T. From the S/N ratio calculations and mean effect plot analyses, four sets of optimal input parameters for the turning process responses (one set per response) will be obtained, which will enable the identification of the optimal turning parameters for each process response separately. Still, it is more beneficial and effective if we can determine one set of optimal input parameters for all the responses investigated simultaneously. For this purpose, multi-criteria decision-making approaches, such as GRA and TOPSIS, can be applied.

3.2 Grey relational analysis

Taguchi's approach to involving an S/N ratio analysis is restricted in its ability to solve optimisation problems that contain multiple objectives. When more than one object is to be resolved, a better alternative is needed. As such, this study attempts to find a solution to the multiple problems that need to be addressed. Hence, Taguchi's approach combined with a GRA was used to determine the optimal cutting conditions in the current study. This combined approach converts multi-objective problems into single-objective problems to discover which combinations of values for various characteristics yield optimal results.

The GRA method is primarily based on the conversion of the multi-response optimisation problem into a single-objective problem. Initially, this method was used to evaluate the performance of a complex project where little information/data is available. At present, this method is widely used to optimise multi-response problems using different machining processes [37, 38]. The present study considers ranks (as opposed to real values) derived from the grey relational grading system. At first, the quality measures considered in the optimisation problem are normalised between zero and one. The normalised data is used to generate a grey relational coefficient (GRC) using appropriate relations. The grey relational grade (GRG), which controls the overall performance characteristics, is then evaluated using the mean of the GRCs of the respective responses. The optimal parametric combination corresponds to the highest value of GRG.

The steps in the GRA method are outlined presently [57, 58]:

STEP 1 The initial step in a GRA is the normalisation of the measured results to values ranging from 0 to 1. This normalisation makes the subsequent analysis simpler and yields more evenly distributed experimental results. The normalisation of data (pre-processing) into a group of sequences is known as a grey relational generation. Which normalisation formula is deemed appropriate depends on the optimisation objective. Before data pre-processing using GRA, the response of the transformed sequences can be categorised into larger-the-better or smaller-the-better quality characteristics. As the present study aims to minimise surface roughness, cutting force, and specific power consumption, the smaller-the-better criterion is

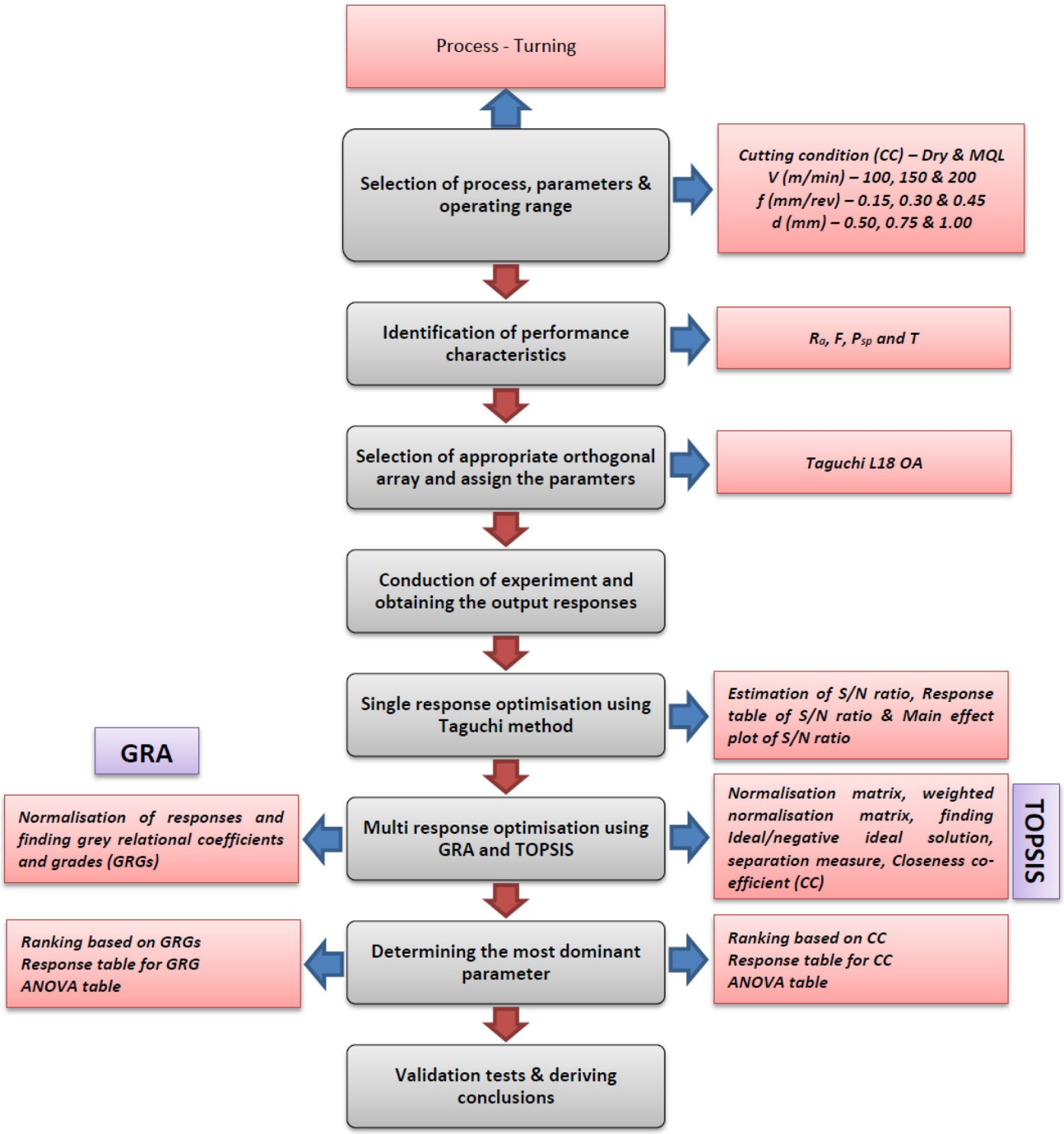

Fig. 4 Flowchart of the current optimisation study

to be adopted. The normalisation expressions for the smaller-the-better are shown in Eq. (4).

$$y_i^*(k) = \frac{\max\left|x_i^0(k)\right| - x_i^0(k)}{\max\left|x_i^0(k)\right| - \min\left|x_i^0(k)\right|} \tag{4}$$

In the above equation, y_i^* is the normalised value, $x_i^0(k)$ is the measured response, i is the number of experiments, and k is the performance characteristic.

STEP 2 After normalising the experimental responses, the next step is to evaluate the GRC; the following expression is used for this purpose:

$$\xi_i(k) = \frac{\Delta_{\min} + \zeta\Delta_{\max}}{\Delta_{0i}(k) + \zeta\Delta_{\max}} \tag{5}$$

In Eq. (5), ξ_i (k) is the GRC, $\Delta_{0i}(k)$ is the offset between the absolute values of the reference sequence $y_0^*(k)$; the comparability sequence $y_i^*(k)$ can be computed as follows:

$$\Delta_{0i}(k) = \left|y_0^*(k) - y_i^*(k)\right| \tag{6}$$

In Eq. (6), ζ is the distinguishing coefficient (the value of which is generally 0.5), and $\Delta_{\min}$ and $\Delta_{\max}$ are the smallest and largest values of Δ_{0i}(k), respectively. The GRC correlates the best, and actual normalised experimental data.

STEP 3 The final step involves estimating the GRGs by taking the average of the GRCs. This can be mathematically expressed as follows:

$$\gamma_i = \frac{1}{n}\sum_{k=1}^{n}\xi_i(k) \tag{7}$$

In the above equation, γ_i is the GRG (the value of which ranges from 0 to 1), and n is the number of experiments.

STEP 4 The next and final step is the prediction and verification of the quality characteristics based on the optimal values calculated using the GRG. The equation below can be used to carry out this step.

$$\gamma_{\text{predicted}} = \gamma_m + \frac{1}{n}\sum_{i=1}^{q}\gamma_o - \gamma_m \tag{8}$$

In Eq. (8), γ_o is the maximum of the average GRG for the optimal levels of factors (as determined in the previous steps), γ_m refers to mean GRG. and q denotes the number of factors that affect the response values.

3.3 Techniques for order preferences by similarity to ideal solution

The TOPSIS study deals with the conversion of a multi-objective problem into a single-objective problem; an optimal parameter combination is chosen based on the closeness of parameter values to coefficient values. In this approach, the solution which is the closest to the positive ideal solution (PIS) and the farthest from the negative ideal solution (NIS) is taken as the optimised solution. The various steps involved in the TOPSIS approach for solving multi-objective characteristics are as follows [50, 59]:

STEP 1 The first step in TOPSIS is the formation of the decision matrix from response variables.

$$X_{ij} = \begin{bmatrix} X_{11} & X_{12} & X_{13} & .. & .. & X_{1n} \\ X_{21} & X_{22} & X_{23} & .. & .. & X_{2n} \\ . & . & . & \ddots & \ddots & . \\ . & . & . & \ddots & \ddots & . \\ . & . & . & \ddots & \ddots & . \\ X_{m1} & X_{m2} & X_{m3} & .. & .. & X_{mn} \end{bmatrix} \tag{9}$$

For $i = 1, 2, 3\ldots m$, $j = 1, 2, 3,\ldots n$, and X_{ij} is the performance measure.

STEP 2 The decision matrix is then normalised using the following relation.

$$r_{ij} = \frac{X_{ij}}{\sqrt{\sum_{i=1}^{m} X_{ij}^2}} \tag{10}$$

In Eq. (10), r_{ij} is the normalised value.

STEP 3 Equal proportions of weights are allocated for each criterion considered. The weighted normalised decision matrix is then formed by multiplying normalised decision matrix by its associated weights.

$$V = W_j r_{ij} \tag{11}$$

W_j represents the weight allocated for each input parameter for $j = 1, 2, 3,\ldots n$. An equal weight is allocated for all output factors so that equal importance is given to all the factors.

STEP 4 Ideal and NISs are found using the equations given below.

The equation used to determine the PIS is

$$A^+ = \left\{V_1^+, \ldots, V_n^+\right\}, \tag{12}$$

where

$$V_j^+ = \left\{\max\left(V_{ij}\right)\text{if}\, j \in J; \min\left(V_{ij}\right)\text{if}\, j \in J'\right\}. \tag{13}$$

The equation used to find the NIS is

$$A^- = \left\{V_1^-, \ldots, V_n^-\right\}, \tag{14}$$

where

$$V_j^- = \left\{\min\left(V_{ij}\right)\text{if}\, j \in J; \max\left(V_{ij}\right)\text{if}\, j \in J'\right\}. \tag{15}$$

STEP 5 The separation measures (i.e. the separation of each alternative) from the PIS and NIS are determined according to Eqs. 16 and 17.

$$S_i^+ = \sum_{i=1}^{m}\sqrt{\left(V_j^+ - V_{ij}\right)^2} \tag{16}$$

$$S_i^- = \sum_{i=1}^{m}\sqrt{\left(V_j^- - V_{ij}\right)^2} \tag{17}$$

STEP 6 A closeness coefficient for each alternative is estimated as per the relation given below.

$$\mathrm{CC} = \frac{S_i^-}{\left(S_i^+ + S_i^-\right)} \quad 0 < \mathrm{CC} < 1 \tag{18}$$

STEP 7 Finally, a TOPSIS ranking is carried out based on the values of the closeness coefficients. A high closeness coefficient indicates that the respective experiment is close to the ideal value.

3.4 Analysis of variance

An ANOVA can determine if the effects that parameters have on certain variables investigated in an experiment are significant. ANOVA tables analyse between-factor interaction and their effects on other variables [60]. This study also used an *F*-test, which measures the extent to which various factors influence the results derived from an ANOVA. For the effect of a factor to be considered statistically significant, the *p* value extracted must be less than 0.05 [61]. A large *F* value means that a factor has a significant effect on regarding a certain outcome.

In an ANOVA, an adjusted correlation coefficient (R^2_{adj}) can determine whether the fitted model is valid by evaluating the percentage of variation that can be accounted for by only the independent variables that significantly affect the dependent variables. It is preferable that there is not much discrepancy between the R^2 and R^2_{adj} values [60, 61].

4 Results and discussion

4.1 Turning test results and Taguchi analysis

The output performance characteristics (i.e. R_a, F, P_{sp}, and T) are measured based on 18 trails; the results are presented in Table 6. GRA and TOPSIS methods are used to optimise the experimental data. First, the experimental data in Table 6 are converted to S/N ratios. As lower values of R_a, F, P_{sp} and T are desirable, the smaller-the-better quality characteristic was selected to investigate the influence of control factors on the multiple responses.

Table 7 Response table for S/N ratios of R_{a}

Level	CC	*V*	*f*	*d*
1	−8.28	−9.39	−4.60	−7.83
2	−7.15	−7.28	−7.67	−7.34
3		−6.47	−10.87	−7.97
Delta	1.12	2.93	6.28	0.63
Rank	3	2	1	4

Table 6 Multi-response results from an S/N-ratio-based Taguchi L18 OA

Trial No.	Designation	Measured responses				S/N ratios of			
		R_a (μm)	F (N)	P_{sp} (N.m/mm^3)	T (°C)	R_a (μm)	F (N)	P_{sp} (N.m/mm^3)	T (°C)
1	A1B1C1D1	2.53	72	1.07	105	−8.06	−37.15	−0.59	−40.42
2	A1B1C2D2	2.95	82	1.11	109	−9.40	−38.28	−0.91	−40.75
3	A1B1C3D3	4.45	108	1.2	134	−12.97	−40.67	−1.58	−42.54
4	A1B2C1D1	1.81	74	1.11	125	−5.15	−37.38	−0.91	−41.94
5	A1B2C2D2	2.12	89	1.15	129	−6.53	−38.99	−1.21	−42.21
6	A1B2C3D3	3.9	112	1.19	152	−11.82	−40.98	−1.51	−43.64
7	A1B3C1D2	1.45	88	1.17	126	−3.23	−38.89	−1.36	−42.01
8	A1B3C2D3	2.5	113	1.22	145	−7.96	−41.06	−1.73	−43.23
9	A1B3C3D1	2.94	110	1.27	137	−9.37	−40.83	−2.08	−42.73
10	A2B1C1D3	1.93	88	1.03	111	−5.71	−38.89	−0.26	−40.91
11	A2B1C2D1	2.77	90	1.03	98	−8.85	−39.08	−0.26	−39.82
12	A2B1C3D2	3.7	94	1.1	122	−11.36	−39.46	−0.83	−41.73
13	A2B2C1D2	1.47	89	1.04	103	−3.35	−38.99	−0.34	−40.26
14	A2B2C2D3	2.32	108	1.07	119	−7.31	−40.67	−0.59	−41.51
15	A2B2C3D1	3	91	1.02	110	−9.54	−39.18	−0.17	−40.83
16	A2B3C1D3	1.27	110	1.06	121	−2.08	−40.83	−0.51	−41.66
17	A2B3C2D1	1.99	99	1.07	112	−5.98	−39.91	−0.59	−40.98
18	A2B3D3C2	3.23	114	1.14	119	−10.18	−41.14	−1.14	−41.51

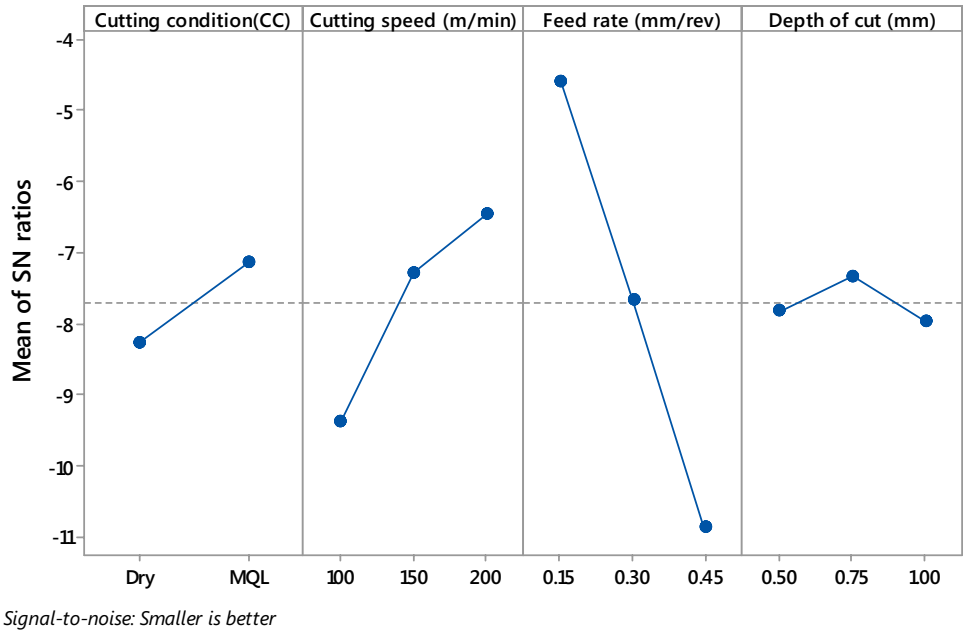

Fig. 5 Main effect plots of S/N ratio for surface roughness

4.2 Effect of control factors on average surface roughness (R_a)

Minitab 18 statistical software is used to convert the experimental data for R_a (shown in Table 6) into S/N ratios. The S/N ratio analysis was used to generate the response table for the S/N ratios of R_a (Table 7); in this table, the delta statistics denote the dominant control factors. The mathematical difference between the highest and the lowest average value of each factor gives the delta value. Ranks are then assigned according to the delta value. The factor with highest delta value is that which predominantly affects R_a; this factor is assigned the first rank. Table 7 indicates that the cutting feed, with a delta value of 6.28, is the most influential factor. The second-most influential factor is cutting speed, with a delta value of 2.93, followed by the cutting condition and depth of cut, having respective delta values of 1.12 and 0.63.

Figure 5 depicts the main effects plot for S/N ratios based on the response data in Table 7. The trend of the plot indicates that R_a is greatly influenced by variations in feed rate. From Table 6, it can be inferred that surface roughness increases as feed rate increases. Further, good surface finish was detected at a low feed rate. This because a low feed rate produces few feed marks on the machined surface, thus reducing the surface roughness. As feed rate increases, the cutting zone temperature increases, causing a decrease in the bonding strength between the matrix metal and reinforcement particles.

So, an increase in feed rate creates more pits and holes on a workpiece's surface. Of the primary reason for this is that Al_2O_3 particles get pulled out from the hybrid composites. These particles then enter the area between the tool and workpiece. The S/N ratios for R_a increase dramatically from 0.15 to 0.45 mm/rev (see Fig. 5). This supports the finding that a low feed rate promotes the quality of response. Figure 5 depicts cutting speed's relationship with S/N ratios. It can be seen that the S/N ratio increases when cutting speed is increased from 100 to 200 m/min. A high cutting speed typically results in a smooth finish on the workpiece's surface. Cutting condition and depth of cut did not have a significant effect of the surface quality of the workpiece in this study. Nevertheless, the combination of the MQL cutting condition and a small depth of cut did reduce the surface roughness of the workpiece, perhaps because the way in which the MQL system removes chips from the cutting area, creating a cool and even cutting surface. As indicated in Fig. 5, the combination of factors that produces the best outcome (i.e. the highest S/N ratio and the lowest R_a) is A2 (which denotes the MQL cutting condition), B3 (which is a cutting speed of 200 m/min), C1 (a feed rate of 0.15 mm/rev), and D2 (a depth of cut of 0.75 mm).

Table 8 Response table for S/N ratios of F

Level	CC	V	f	d
1	− 39.36	− 38.92	− 38.69	− 38.92
2	− 39.79	− 39.37	− 39.67	− 39.29
3		− 40.44	− 40.38	− 40.52
Delta	0.44	1.52	1.69	1.59
Rank	4	3	1	2

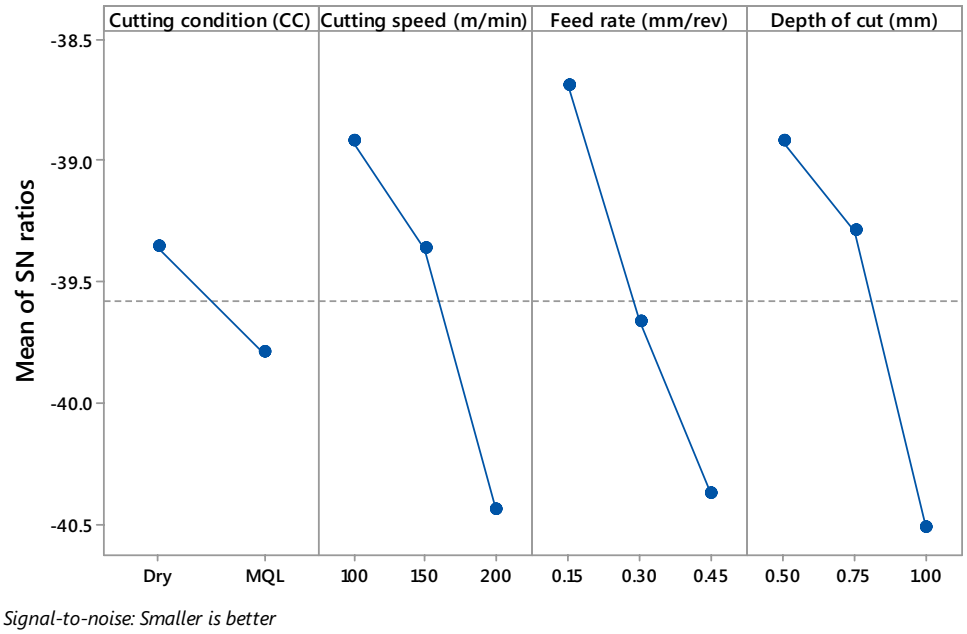

Fig. 6 Main effect plots of S/N ratio for cutting force

4.3 Effect of control factors on cutting force (*F*)

Table 6 shows the calculated S/N ratio values for the experimental data. The smaller-the-better characteristic of the Taguchi method was also adopted here, and the response table based on the Taguchi analysis is presented in Table 8. It was discovered that feed rate (delta = 1.69) has the most drastic effect on *F*. Depth of cut (delta = 1.59) was the second-most effective factor, followed by cutting speed (delta = 1.52) and cutting condition (delta = 0.44).

From the main effects plot for S/N ratios of *F* (Fig. 6), feed rate, depth of cut, and cutting speed are detected as the variables that are the most influential on cutting force, while the cutting condition did not have a significant effect. An increase in feed rate increases the MRR, and consequently, more cutting force is required to cut the material. With an increase in the depth of the cut, a greater portion of the workpiece comes into contact with the tool—to remove this greater amount of material, more cutting force needs to be applied. Thus, we can conclude that cutting force can be reduced if the feed rate is lowered and if the depth of cut is minimised.

Figure 6 also depicts the influence that cutting speed has on cutting force. Maximum cutting force is associated with high cutting speeds. Normally, the cutting zone temperature increases at high cutting speeds, causing more flank wear on the tool surface, thus reducing the cutting efficiency of the tool. Hence, more cutting force is required for the tool to cut through the workpiece. Though a workpiece undergoes thermal softening when temperature is increased, the existence of Al_2O_3 particles (which can withstand high temperatures without softening) in the workpieces employed in this study acts as a barrier in reducing the cutting force.

Cutting condition has the least impact on cutting force. Though the application of MQL requires a lower cutting force than dry cutting, this was not the case in every trial. Other researchers also reported similar results [38, 62]. Viswanathan et al. [38] conducted turning experiments on AZ91D Mg alloy in dry and MQL condition and suggested dry cutting condition over MQL to achieve minimum cutting force. Similar observation was also reported in the study of Eker et al. [62] in which he was able to obtain a reduction of approximately 3.6% in dry condition when compared to MQL condition. The optimum condition for minimal cutting force is a cutting speed of 100 m/min, a feed rate of 0.15, and a depth of cut of 0.5 mm under the dry cutting condition.

The cutting condition usually has an effect on the cutting temperature rather than cutting force. In dry cutting, at higher cutting speeds, heat generates at an accelerated rate causing a temperature rise. Consequently, an increase in friction causes cold-welding of the chip on the tool face and thus a new geometry is formed on the cutting edge of the tool called build-up edge (BUE). BUE increases the effective

Table 9 Response table for S/N ratios of P_{sp}

Level	CC	*V*	*f*	*d*
1	−1.32	−0.74	−0.66	−0.76
2	−0.52	−0.79	−0.88	−0.97
3		−1.23	−1.22	−1.03
Delta	0.80	0.50	0.56	0.26
Rank	1	3	2	4

rake angle of the tool, and thus less energy is consumed for cutting. But in MQL machining, tendency for BUE formation is minimum as lubricant disposes the chips away from the cutting zone. Hence, the reduction in energy consumption by increasing the effective rake angle is not achieved. However, the cutting fluid provides a cooling effect and thus heat generated drops. Further, under the lubrication condition, it was reported that when cutting speed increases, chip sweeps the lubricant away from the chip-tool interface through a hydrodynamic action while moving parallel to the face of the tool [63]. Hence, the lubricant becomes less effective in the chip-workpiece interface at higher cutting speeds [64]. Tool wear is another reason causing higher cutting force requirement in MQL conditions at high speed.

4.4 Effect of control factors on specific power consumption (P_{sp})

Table 9 is the response table based on the S/N ratio analysis of P_{sp}. As the table indicates, the cutting condition is considered the most dominant factor in terms of its influence on specific power, as it has a delta value of 0.80. Feed rate is the second-most significant factor, with a delta of 0.56. Cutting speed (delta = 0.50) and depth of cut (delta = 0.26) were the third-most and least influential factors. Figure 7 shows the main effects plot for the S/N ratios of P_{sp}. A close examination of Table 9 and Fig. 7 reveals that there is little variation among the delta values of each of the four control factors; thus, each factor has nearly the same impact on P_{sp} as the other factors.

An increase in feed rate increases tool flank wear, causing a reduction in the cutting ability of the tool. Consequently, more specific power is required to cut the material. An increase in the depth of cut requires the tool to be in contact with the workpiece for a longer time. Hence, the machining process requires greater cutting force and cutting power to remove a unit volume of material as the depth of the cut increases. As cutting force increases at higher speeds due to the presence of Al_2O_3 particles (which can withstand high temperatures without being softened), specific power consumption also increases with an increase in cutting speed from 100 to 200 m/min. The depth of the cut has the least influence on specific power. Overall, the variation in the delta values among all the control factors is minimal. The ideal condition for minimal specific power is a cutting speed of 100 m/min, a feed rate of 0.15 mm/rev, and a depth of cut of 0.5 mm under the MQL cutting condition.

Generally, the power consumption results are in parallel with the cutting force values. In this study, however, the cutting forces were higher in MQL cutting conditions than in dry cutting conditions, while the power consumption values were lower in MQL cutting conditions. Similar results in which power consumption and cutting forces behave differently under MQL condition were also reported recently [65].

4.5 Effect of control factors on cutting zone temperature (*T*)

The response table based on S/N ratio analysis and main effects plot for S/N ratios of *T* are shown in Fig. 8 and Table 10. From these results, it was found that the most dominant factor influencing T was cutting condition, with a delta value of 1.14. Cutting condition is followed by depth of cut, cutting speed, and feed rate. However, there were no

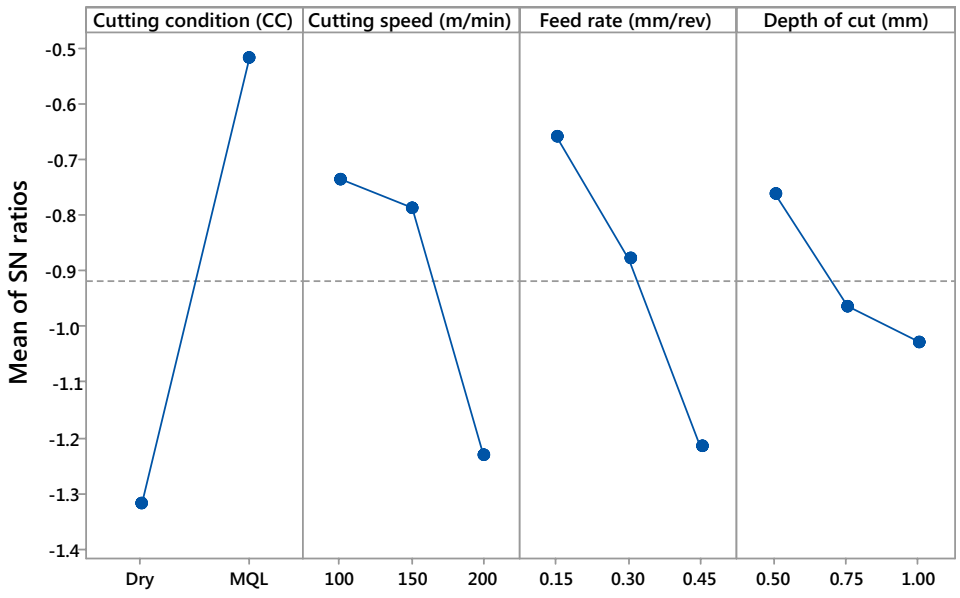

Fig. 7 Main effect plots of S/N ratios for specific power consumption

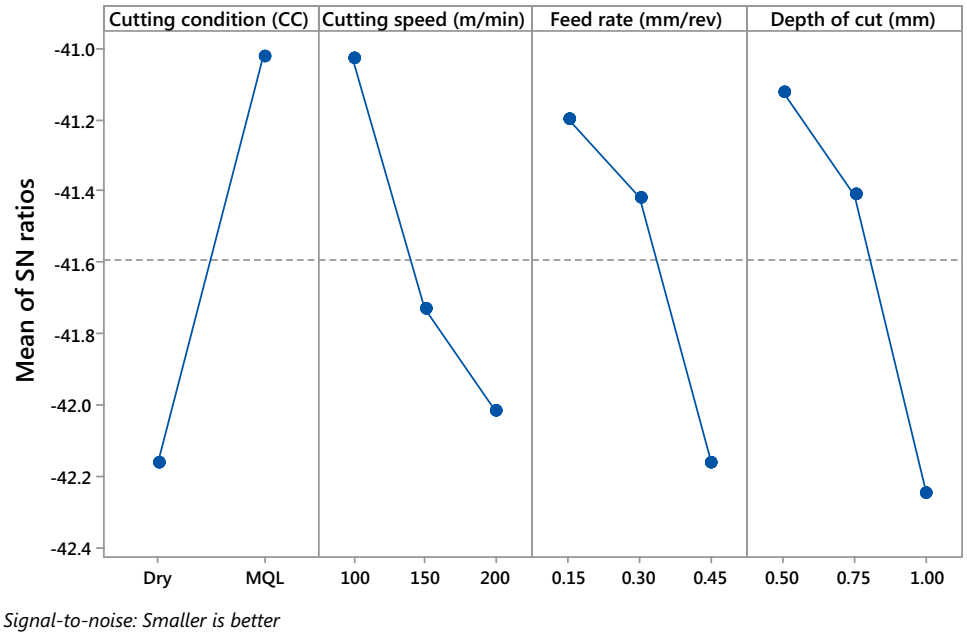

Fig. 8 Main effect plots of S/N ratio for cutting zone temperature

Table 10 Response table for S/N ratios of T

Level	CC	V	f	d
1	−42.16	−41.03	−41.2	−41.12
2	−41.02	−41.73	−41.42	−41.41
3		−42.02	−42.16	−42.25
Delta	1.14	0.99	0.97	1.12
Rank	1	3	4	2

major variations detected between the delta values of these factors, indicating that they all have a similar impact on cutting zone temperature.

Figure 8 shows that increases in cutting speed, feed rate, and depth of cut increase the temperature required for the machining of Mg MMCs, as increases in these variables mean that more force is required to cut the workpiece. When the spindle speed is increased, it causes energy to dissipate more quickly from plastic deformation and friction. Thus, the generation of heat in the cutting area rises. This, naturally, creates a high cutting temperature [66].

An increase in feed rate also causes the temperature to rise more quickly in the cutting zone. Furthermore, when a deep cut needs to be made, more material needs to be removed by the tool; the consequential increased contact between the tool and the workpiece causes the temperature of the cutting area to rise. In addition, when a tool makes a deep cut, more particles of the workpiece will adhere to the tool than when a shallow cut is made. The presence of extra workpiece particles on the tool further increases the temperature of the cutting zone [67]. The temperature of the cutting zone, as well as the amount of heat generated via the cutting process, can be decreased by using cutting fluids. The results of this study show that the coolest cutting zone temperature is achieved with a cutting speed of 100 m/min, a feed rate of 0.15 mm/rev, and a depth of cut of 0.5 mm under the MQL cutting condition.

Once the effects of the parameters on responses have been analysed, the relationships that are found among the responses need to be understood in more detail, as some of the relationships depend on other relationships. Moreover, in real-world applications, the optimal combination of parameters for multiple responses needs to be determined. As such, a GRA and TOPSIS were employed for the multi-response optimisation in this study considering the various factors and responses.

4.6 Multi-objective optimisation via grey relational analysis

By employing a GRA, certain problems can be solved even when the amount of available data is limited. Generally, a GRA is utilised to determine outcomes for which there is no clear solution. In a GRA, the term ‘black’ denotes the absence of information, while the term ‘white’ indicates that all relevant information is present [47]. As part of the data pre-processing stage, GRG was utilised using as per the experimental data given in Table 6 for R_a, F, P_{sp}, and T. The values of all responses were normalised within the range of 0–1; this was accomplished via Eq. (4). After the data was normalised, Eq. (6) was used to compute the deviation sequences.

In Table 11, the reference and deviation sequences that were obtained through data pre-processing can be observed.

Table 11 Reference and deviation sequences after data pre-processing

Trial No.	Reference sequence (y_i^*)				Deviation sequence (Δ_{0i})			
	R_a	F_y	P_{sp}	T	R_a	F_y	P_{sp}	T
1	0.604	1.000	0.800	0.870	0.396	0.000	0.200	0.130
2	0.472	0.762	0.640	0.796	0.528	0.238	0.360	0.204
3	0.000	0.143	0.280	0.333	1.000	0.857	0.720	0.667
4	0.830	0.952	0.640	0.500	0.170	0.048	0.360	0.500
5	0.733	0.595	0.480	0.426	0.267	0.405	0.520	0.574
6	0.173	0.048	0.320	0.000	0.827	0.952	0.680	1.000
7	0.943	0.619	0.400	0.481	0.057	0.381	0.600	0.519
8	0.613	0.024	0.200	0.130	0.387	0.976	0.800	0.870
9	0.475	0.095	0.000	0.278	0.525	0.905	1.000	0.722
10	0.792	0.619	0.960	0.759	0.208	0.381	0.040	0.241
11	0.528	0.571	0.960	1.000	0.472	0.429	0.040	0.000
12	0.236	0.476	0.680	0.556	0.764	0.524	0.320	0.444
13	0.937	0.595	0.920	0.907	0.063	0.405	0.080	0.093
14	0.670	0.143	0.800	0.611	0.330	0.857	0.200	0.389
15	0.456	0.548	1.000	0.778	0.544	0.452	0.000	0.222
16	1.000	0.095	0.840	0.574	0.000	0.905	0.160	0.426
17	0.774	0.357	0.800	0.741	0.226	0.643	0.200	0.259
18	0.384	0.000	0.520	0.611	0.616	1.000	0.480	0.389

Table 12 Grey relational coefficients, grades S/N ratios and rank

Trial No.	Grey relational coefficient (ξi (k))				Grey relational grade (γi)	S/N Ratio of GRG	Rank
	R_a	F_y	P_{sp}	T			
1	0.558	1.000	0.714	0.794	0.767	−2.30	2
2	0.486	0.677	0.581	0.711	0.614	−4.24	9
3	0.333	0.368	0.410	0.429	0.385	−8.29	17
4	0.746	0.913	0.581	0.500	0.685	−3.29	5
5	0.652	0.553	0.490	0.466	0.540	−5.35	12
6	0.377	0.344	0.424	0.333	0.370	−8.64	18
7	0.898	0.568	0.455	0.491	0.603	−4.39	10
8	0.564	0.339	0.385	0.365	0.413	−7.68	15
9	0.488	0.356	0.333	0.409	0.397	−8.02	16
10	0.707	0.568	0.926	0.675	0.719	−2.87	4
11	0.515	0.538	0.926	1.000	0.745	−2.56	3
12	0.396	0.488	0.610	0.529	0.506	−5.92	13
13	0.888	0.553	0.862	0.844	0.787	−2.08	1
14	0.602	0.368	0.714	0.563	0.562	−5.01	11
15	0.479	0.525	1.000	0.692	0.674	−3.43	6
16	1.000	0.356	0.758	0.540	0.663	−3.57	7
17	0.688	0.438	0.714	0.659	0.625	−4.08	8
18	0.448	0.333	0.510	0.563	0.463	−6.69	14

Equation (5) was used to calculate the GRCs (ξ_i (k)) for all response values after the deviation sequences had been determined. Lastly, the average value of all calculated GRCs was computed to arrive at the GRG (γ_i). Table 12 displays the GRGs that were used to produce the corresponding S/N ratios. High S/N ratios are desirable, as such ratios signal that the experimental data is close to the ideal normalised GRG value [68].

The plot comparing the GRGs to S/N ratios is displayed in Fig. 9 and is a supplement to the results provided by Table 12. This plot reveals that the highest S/N ratio was obtained during the thirteenth experimental run. As such, the thirteenth run was assigned the first rank.

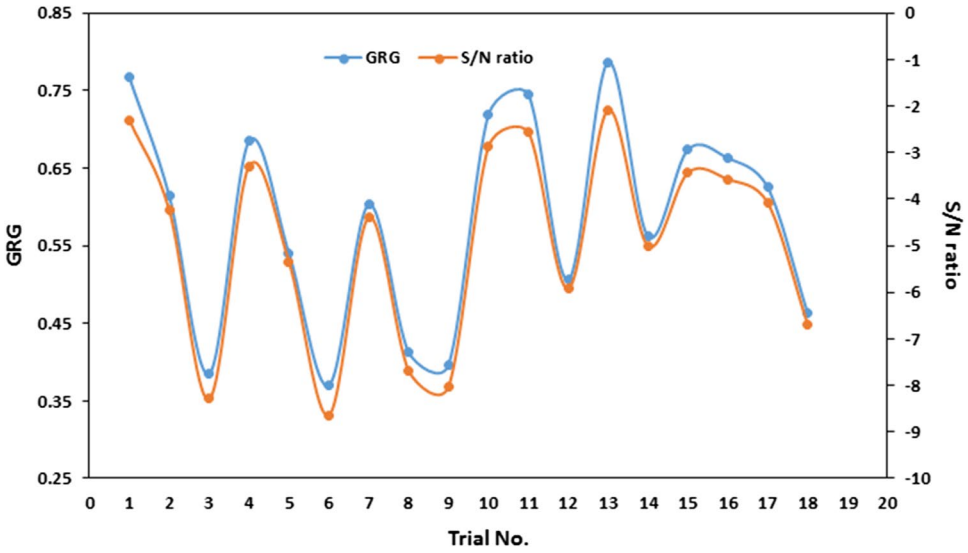

Fig. 9 Plot of GRG versus S/N ratios

Table 13 Response table for GRG

Level	Cutting condition (A)	Cutting speed (B)	Feed rate (C)	Depth of cut (D)
1	0.530	**0.623**	**0.704**	**0.649**
2	**0.638**	0.603	0.583	0.586
3		0.527	0.466	0.519
Delta	0.108	0.095	0.238	0.130
Rank	3	4	1	2

The optimal combinations are marked in bold letters

Total mean grey relational grade = 0.5905

A GRG response table was constructed after all ranks were determined. A mean GRG for each factor was calculated through the selection and averaging the GRGs at chosen levels. To give an example, cutting speed was set at level 1 for the first, second, third, tenth, eleventh, and twelfth experimental runs. The appropriate GRG values, as dictated by the data in Table 12, were used in the calculation as per Eq. (19).

$$V(\text{Level1}) = \frac{0.767 + 0.614 + 0.387 + 0.719 + 0.745 + 0.506}{6} = 0.623 \quad (19)$$

The procedure outlined above was used to compute the mean value of the chosen GRGs. After this computation, the response table (Table 13) was created. The grades delineated in Table 13 indicate the level of correlation between the reference and comparability sequences of

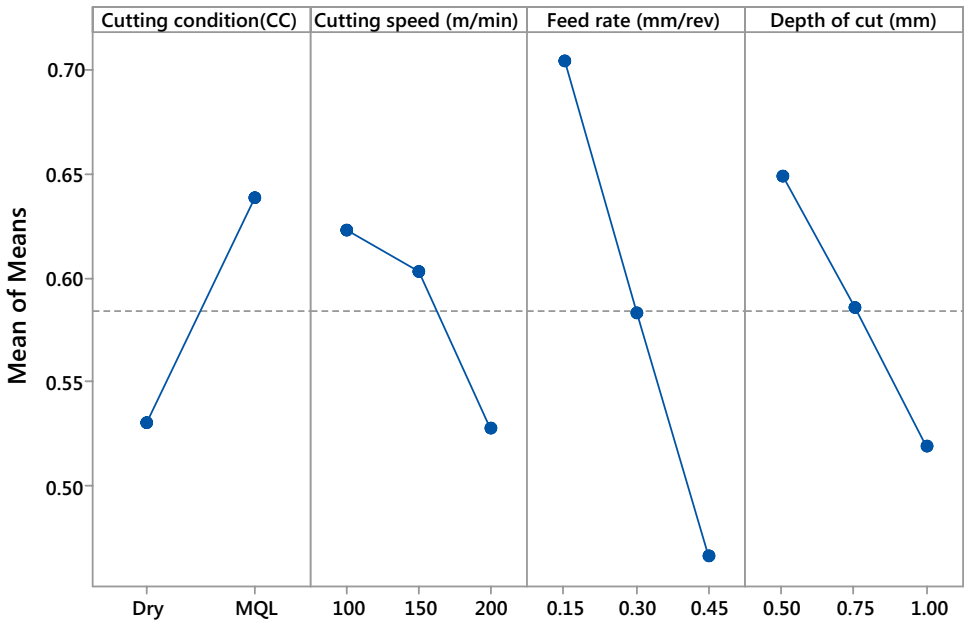

Fig. 10 Main effect plot of means for GRG

Table 14 Results of ANOVA analysis for GRGs

Factors	DF	Seq SS	Adj MS	*F* Value	*P* Value	Contribution (%)
Cutting condition	1	0.05084	0.05084	33.99	0	15.93
Cutting speed	2	0.03040	0.01520	9.88	0.004	9.53
Feed rate	2	0.17018	0.08509	55.33	0	53.33
Depth of cut	2	0.05227	0.026135	16.53	0.001	16.38
Error	10	0.01538	0.001538			4.82
Total	17	0.31908			$R^2 = 95.18\%$	$R^2_{adj} = 91.81\%$

Table 15 Normalised and weighted normalised values of output responses

Trial No.	R_a		F		P_{sp}		T	
	NM	WNM	NM	WNM	NM	WNM	NM	WNM
1	0.220	0.044	0.175	0.035	0.226	0.045	0.203	0.041
2	0.256	0.051	0.199	0.040	0.234	0.047	0.211	0.042
3	0.387	0.077	0.262	0.052	0.253	0.051	0.259	0.052
4	0.157	0.031	0.180	0.036	0.234	0.047	0.242	0.048
5	0.184	0.037	0.216	0.043	0.243	0.049	0.250	0.050
6	0.339	0.068	0.272	0.054	0.251	0.050	0.294	0.059
7	0.126	0.025	0.214	0.043	0.247	0.049	0.244	0.049
8	0.217	0.043	0.274	0.055	0.258	0.052	0.281	0.056
9	0.255	0.051	0.267	0.053	0.268	0.054	0.265	0.053
10	0.168	0.034	0.214	0.043	0.218	0.044	0.215	0.043
11	0.241	0.048	0.219	0.044	0.218	0.044	0.190	0.038
12	0.321	0.064	0.228	0.046	0.232	0.046	0.236	0.047
13	0.128	0.026	0.216	0.043	0.220	0.044	0.199	0.040
14	0.202	0.040	0.262	0.052	0.226	0.045	0.230	0.046
15	0.261	0.052	0.221	0.044	0.215	0.043	0.213	0.043
16	0.110	0.022	0.267	0.053	0.224	0.045	0.234	0.047
17	0.173	0.035	0.240	0.048	0.226	0.045	0.217	0.043
18	0.281	0.056	0.277	0.055	0.241	0.048	0.230	0.046

the GRA. The higher the mean GRG value, the stronger the correlation [38]. Thus, it can be concluded from the data in Table 13 that achieving an optimal combination of parameters (i.e. a combination that leads to the maximum overall response) is possible. As indicated in Table 13, the maximum GRGs values are achieved at A2 (CC at level 2), B1 (V at level 1), C1 (f at level 1), and D1 (d at level 1). Accordingly, it can be concluded that the optimum combination for the turning of Mg-based composites is present when the MQL cutting condition is employed with a cutting speed of 100 m/min, a feed rate of 0.15 mm/rev, and a depth of cut of 0.5 mm. This result is represented visually in Fig. 10. The optimised set of parameters lies outside Taguchi's L18 experimentation. The results obtained are similar to those provided by Eker et al. [38, 62].

An ANOVA for GRG at a 95% confidence interval was utilised to determine the significance and the percentage contribution of the investigated factors on the observed performance characteristics of the Mg-3.0Zn-0.7Zr-1.0Cu alloy-based hybrid Al_2O_3 composite. The results of this

Table 16 Positive and negative ideal solution for output responses

	R_a	F	P_{sp}	T
V^+	0.022	0.035	0.043	0.038
V^-	0.077	0.055	0.054	0.059

ANOVA revealed that every factor had a significant effect on the performance characteristics (that is, all p values were < 0.05). A sequential sum of square values was used to calculate the contribution percentage of each factor. It was found that feed rate had the most on GRG influence (53.33%). Depth of cut was the second-most influential factor (16.38%). This was followed by cutting condition (15.93%), and, finally, by cutting speed (9.53%). As mentioned in the corresponding table, when R^2 is close to the unity value (95.18% or 0.9518), this means that this value is significant according to the ANOVA (Table 14).

Table 17 Separation measure, closeness coefficient, and ranking based on CC for various experimental runs

Trial No	Si^+	Si^-	CC	Rank
1	0.022	0.044	0.665	8
2	0.030	0.035	0.539	11
3	0.060	0.008	0.119	18
4	0.015	0.051	0.779	3
5	0.021	0.043	0.670	7
6	0.054	0.010	0.158	17
7	0.015	0.055	0.784	2
8	0.035	0.034	0.490	13
9	0.039	0.027	0.408	14
10	0.015	0.049	0.770	4
11	0.027	0.039	0.587	10
12	0.045	0.021	0.322	16
13	0.009	0.057	0.862	1
14	0.027	0.040	0.601	9
15	0.032	0.034	0.515	12
16	0.021	0.057	0.736	5
17	0.019	0.047	0.711	6
18	0.041	0.025	0.383	15

Table 18 Response table for CC

Level	Cutting condition (A)	Cutting speed (B)	Feed rate (C)	Depth of cut (D)
1	0.512	0.500	**0.766**	**0.611**
2	**0.610**	**0.597**	0.600	0.593
3		0.585	0.318	0.479
Delta	0.097	0.097	0.448	0.132
Rank	3	4	1	2

The optimal combinations are marked in bold letters

4.7 Multi-objective optimisation via TOPSIS

Equations (10)–(18) are used to estimate the closeness coefficient (CC) for each alternative from the response variables. Normalisation was achieved using Eq. (10), and equal weights method was employed in the present research to assign weights. In equal weights method, equal weights (weight for each attribute is calculated by dividing 1 by the total number of attributes) were provided to the response variables to calculate the weight normalised. The normalised matrix (NM) and weighted normalisation matrix (WNM) were then determined by consolidating the values corresponding to each response variable, which were then formed into a table (Table 15). Table 16 shows the PISs and NISs identified for each response. From these ideal solutions, separation measures were found using the relations given in Eqs. 16 and 17.

Table 17 shows the estimated separation measures and CC values for each experimental run. The rankings are based on the descending order of CC values. A high CC value is an indication that the respective experiment is closer to the ideal value. Referring to the CC values and their rankings, experimental trial 13 contained the optimal conditions, as it resulted in the highest CC value among all 18 experimental trials. Conversely, trial 3 displayed the lowest closeness value and proved to be the least desirable choice for machining. A response table for CC (TOPSIS) is further constructed to obtain the optimised set of parameters using the same principle as was used in formulating the response table for GRA.

From the response table for CC (Table 18), it can be observed that level 1 for feed rate and depth of cut form the optimised set of input parameters (i.e. the experimental trial with highest CC) according to TOPSIS (i.e. a cutting speed of 150 m/min, a feed rate of 0.15 mm/rev, and a depth of cut of 0.5 mm under the MQL cutting condition). The optimal combination is marked in bold letters in the response table, and the same is graphically represented in Fig. 11. Also, the optimised set of parameters is found to fit outside Taguchi's L18 experimentation.

The ANOVA for CC (see Table 19) denotes that all the input parameters considered, except for cutting speed, had a significant effect on the output responses (i.e. p values are < 0.05 at a 95% confidence level). Individual sequential sum of square values and their total sum were used to calculate each parameter's percentage contribution to the response variables; the result shows that feed rate has highest influence (78.35%) on CC, followed by depth of cut (7.82%), cutting condition (5.40%), and cutting speed (4.26%). The R^2 value given in Table 19 is nearly equal to unity (95.84%, or 0.9584), thus proving the significance of ANOVA for CC.

4.8 Prediction of R_a, F, P_{sp} and T

Response models for surface roughness, cutting force, specific power, and cutting temperature were predicted under dry and MQL conditions through a general regression method. Equations are developed based on the results of turning operations conducted on Mg hybrid MMC to be used to plot the graphs comparing the experimental and predicted values. The equations obtained for R_a, F, P_{sp}, and T (depending on the V, f, and d) are as follows:

$$R_a = 1.686 - 0.00825V + 5.978f + 0.443d \tag{20}$$

$$F = 27.42 + 0.1667V + 60.0f + 34.33d \tag{21}$$

$$P_{sp} = 0.8931 + 0.000650V + 0.244f + 0.0667d \tag{22}$$

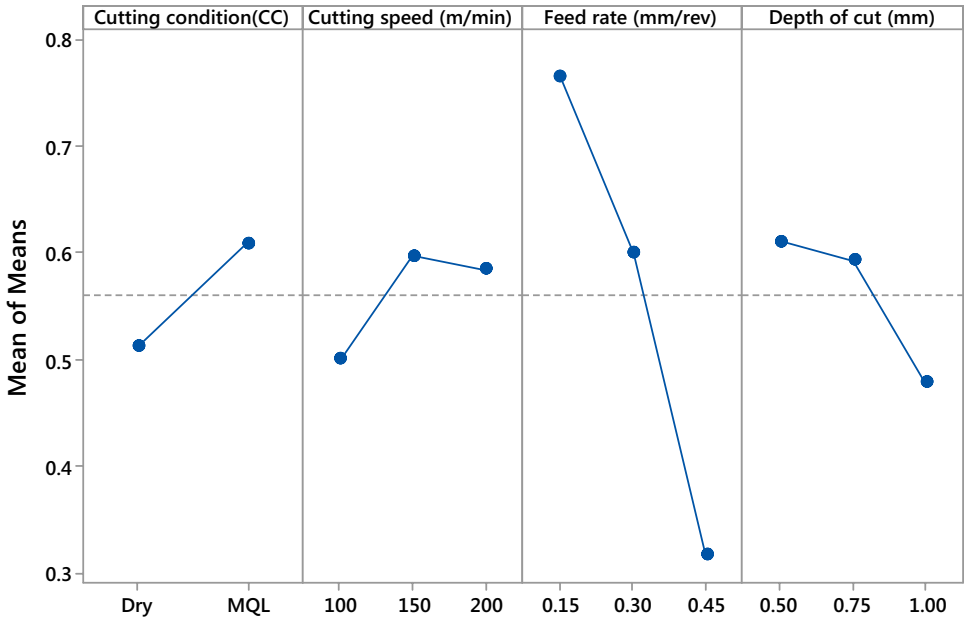

Fig. 11 Main effect plot of means for CC

Table 19 Results of ANOVA analysis for CC

Factors	DF	Seq SS	Adj MS	*F* Value	*P*-Value	Contribution (%)
Cutting condition	1	0.04251	0.042507	12.99	0.005	5.40
Cutting speed	2	0.03354	0.016769	5.13	0.029	4.26
Feed rate	2	0.61632	0.308162	94.2	0	78.35
Depth of cut	2	0.0615	0.030748	9.4	0.005	7.82
Error	10	0.03271	0.003271			4.16
Total	17	0.78658			$R^2 = 95.84\%$	$R^2_{adj} = 92.93\%$

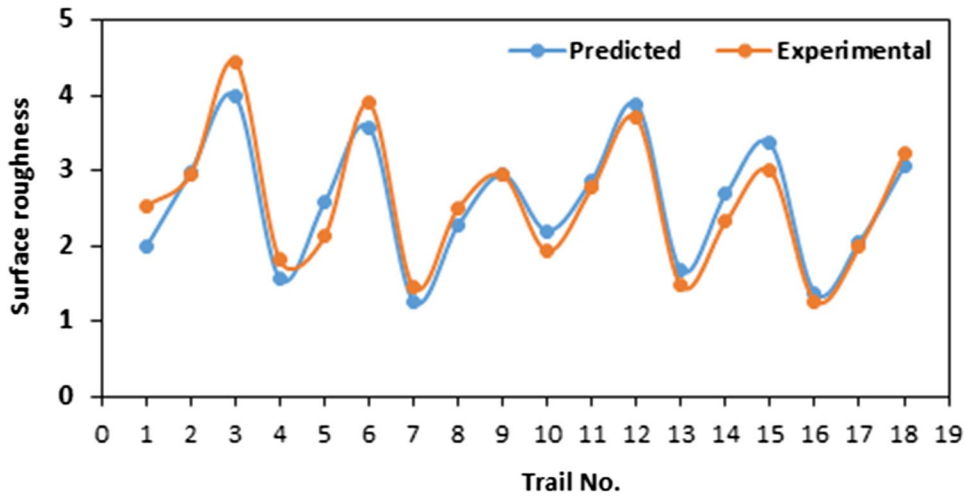

Fig. 12 Experimental versus predicted in-surface roughness

$$T = 63.1 + 0.1350V + 46.1f + 31.7d \quad (23)$$

Graphs comparing the experimental results and predicted values from the regression model for surface roughness, cutting force, specific power and cutting temperature values are shown in Figs. 12, 13, 14 and 15. The graphical results reveal that the predicted values of each response variable are almost in agreement with the experimental results; thus, the developed regression model can be used to predict the response variables for the turning of Mg/μ.Al_2O_3/n.Al_2O_3 hybrid MMCs.

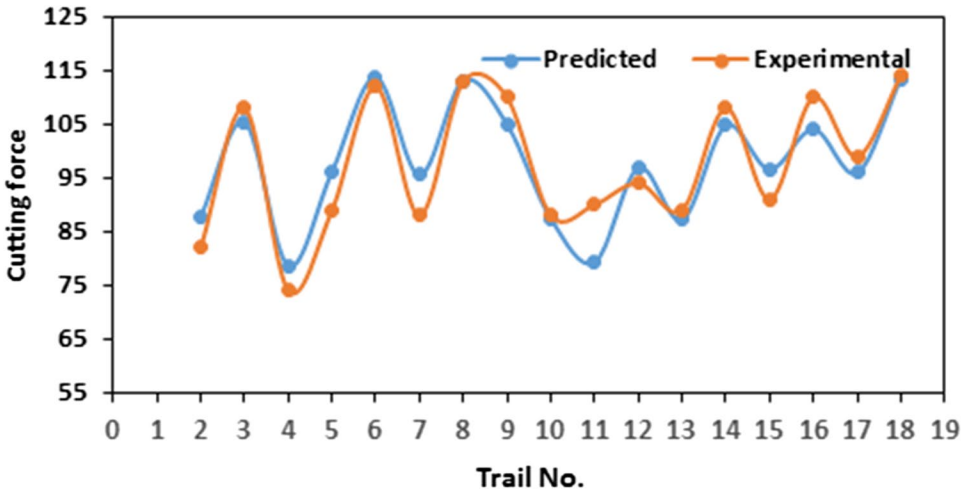

Fig. 13 Experimental versus predicted in-cutting force

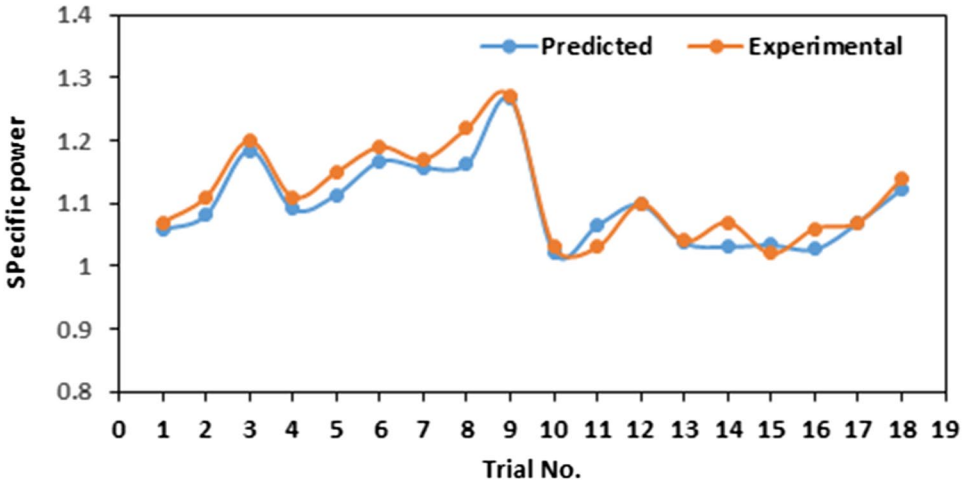

Fig. 14 Experimental versus predicted in-specific power consumption

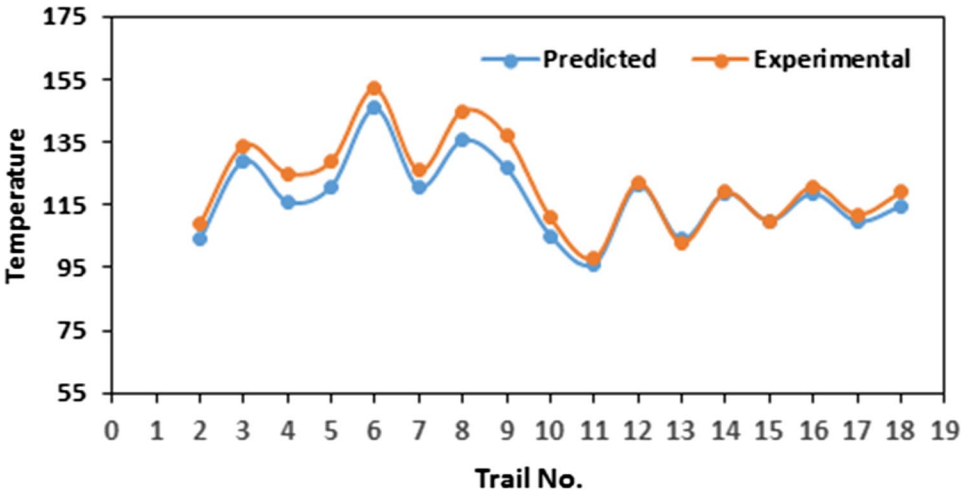

Fig. 15 Experimental versus predicted in-cutting zone temperature

Table 20 Validation test results by grey relation-based Taguchi optimisation

Setting level	Initial setting	TOPSIS	
		Prediction	Experiment
	A1B1C2D2	A2B2C1D1	A2B2C1D1
R_a in µm	2.95		1.47
F in N	82		79
P_{sp} in N.m/mm^3	1.11		1.06
T in °C	109		106
CC	0.539	0.923	0.905
Improvement in CC	–	0.384	0.366

4.9 Comparison of GRA, TOPSIS, and confirmation test results

The analysis of the response table and mean effect plots reveal that the results from both the GRA and TOPSIS optimisation fall outside Taguchi's L18 experimental run. Moreover, the two approaches conclude with different sets of optimal parameter combinations. So, to find the optimal combination from GRA and TOPSIS results while validating the analysis, GRA and CC values are predicted using the relation given in Eq. (8).

The prediction results revealed that the predicted closeness value of the TOPSIS (0.923) is higher than that of the GRA (0.842). Based on the prediction results, the optimised set of parameters obtained from the TOPSIS is used to conduct the confirmation test. The confirmation test results are shown in Table 20, and they are in good agreement with the predicted values. A closeness value of 0.905 was also found; this result is better than that Taguchi's L18 OA. Additionally, an improvement of 36.6% in CC (when compared to the initial parameter setting) was achieved. The results of the validation tests (improved experimental results over the initial design parameters) also affirm the validity of the Taguchi method coupled with TOPSIS for enhancing the performance measures of Mg hybrid composites. The optimisation results agree with the findings of previous studies [38, 65].

5 Conclusions

This paper aimed to optimise the performance characteristics (i.e. surface roughness, cutting force, specific power consumption, and cutting temperature) during the turning of a newly developed Mg/µ.Al_2O_3/n.Al_2O_3 hybrid MMC under dry and MQL conditions. A PM process was used to synthesise the Mg-based hybrid MMC. Taguchi's L18 OA was used to perform the turning experiments, and through a regression analysis, the modelling and prediction of performance measures were completed. GRA and TOPSIS approaches were employed to perform the multi-objective optimisation process. The conclusions derived from the experiment results and subsequent analysis are as follows.

- The optimised set of parameters from both GRA and TOPSIS fit outside Taguchi's L18 experimentation. Further, the GRA and TOPSIS yielded different sets of parameter combinations. Hence, the predicted closeness value was calculated for both methods, and it was noted that the predicted closeness value of the TOPSIS is greater than the predicted GRG value of the GRA. Accordingly, the confirmation test was based on the TOPSIS optimised parameter combination. The test results agreed with the actual results.
- The optimised parameter combinations obtained using TOPSIS were as follows: cutting condition = MQL, cutting speed = 150 m/min, feed rate = 0.15 mm/rev, depth of cut 0.50 mm. The corresponding output response values were as follows: surface roughness = 1.47 µm, cutting force = 79 N, specific power consumption = 1.06 in Nm/mm3, cutting zone temperature = 106 °C.
- ANOVA results of both GRG values and TOPSIS relative closeness values indicated that feed rate had the greatest effect on the overall objective, while cutting speed had the least influence on the output responses.
- The optimum cutting conditions yielded an improvement in CC from 0.539 to 0.905. Generally, the MQL system provides much better results than those obtained through dry machining. It has been confirmed that this finding has a close relationship with the results obtained by Rubio et al. [23] and Viswanathan et al. [38].

The results derived from the present study indicate that better performance while turning Mg hybrid MMC is achieved during MQL lubrication. Further, MQL machining had great impact on reducing the temperature developed in the cutting zone and this eventually improves the operating life of the tool. Still, an improvement in productivity and quality of machined surface is possible in MQL machining. Based on that motive, future studies can be done to optimise the amount of MQL lubrication. Influence of the MQL lubrication on other unexposed output parameters (for, e.g. tool wear) can also be investigated with further experiments.

Acknowledgements Authors would like to acknowledge the facilities, scientific and technical assistance from Vidya Academy of Science and Technology, Thrissur, Kerala and NICHE, Kumaracoil, Tamil Nadu.

Data availability The raw/processed data required to reproduce these findings cannot be shared at this time as the data also forms part of an ongoing study.

Funding information This research did not receive any specific grant from funding agencies in the public, commercial, or not-for-profit sectors.

Compliance with ethical standards

Conflicts of interest Authors have no conflicts of interest.

References

1. Beck AV (ed) (1943) The technology of magnesium and its alloys. FA Hughes & Company Limited, London
2. Hirsch J, Al-Samman T (2013) Superior light metals by texture engineering: optimized aluminum and magnesium alloys for automotive applications. Acta Mater 61(3):818–843
3. Thein MA, Lu L, Lai MO (2009) Effect of milling and reinforcement on mechanical properties of nanostructured magnesium composite. J Mater Process Technol 209(9):4439–4443
4. Kainer KU, Dieringa H, Dietzel W, Hort N, Blawert C (2006) The use of magnesium alloys: past, present and future. In: Proceedings of the magnesium technology in the global age, international symposium, COM 2006, 45th annual conference of metallurgists of CIM, Montreal, CN, 1–4 Oct 2006. Fraunhofer IRB Verlag, Stuttgart, pp 3–19. ISBN: 1-894475-66-6
5. Bettles C, Gibson M (2005) Current wrought magnesium alloys: strengths and weaknesses. J Mater 57(5):46–49
6. Suneesh E, Sivapragash M (2018) Comprehensive studies on processing and characterization of hybrid magnesium composites. Mater Manuf Process 33(12):1324–1345
7. Eacherath S, Murugesan S (2018) Synthesis and characterization of magnesium-based hybrid composites—a review. Int J Mater Res 109(7):661–672
8. Goh CS, Wei J, Lee LC, Gupta M (2005) Development of novel carbon nanotube reinforced magnesium nanocomposites using the powder metallurgy technique. Nanotechnology 17(1):7
9. Kvashnin DG, Krasheninnikov AV, Shtansky D, Sorokin PB, Golberg D (2016) Nanostructured BN–Mg composites: features of interface bonding and mechanical properties. Phys Chem Chem Phys 18(2):965–969
10. Wang XJ, Wang NZ, Wang LY, Hu XS, Wu K, Wang YQ, Huang YD (2014) Processing, microstructure and mechanical properties of micro-SiC particles reinforced magnesium matrix composites fabricated by stir casting assisted by ultrasonic treatment processing. Mater Des 57:638–645
11. Sankaranarayanan S, Habibi MK, Jayalakshmi S, Jia Ai K, Almajid A, Gupta M (2015) Nano-AlN particle reinforced Mg composites: microstructural and mechanical properties. Mater Sci Technol 31(9):1122–1131
12. Lloyd DJ (1994) Particle reinforced aluminium and magnesium matrix composites. Int Mater Rev 39(1):1–23
13. Ibrahim IA, Mohamed FA, Lavernia EJ (1991) Particulate reinforced metal matrix composites—a review. J Mater Sci 26(5):1137–1156
14. Zhang Z, Han BQ, Witkin D, Ajdelsztajn L, Laverna EJ (2006) Synthesis of nanocrystalline aluminum matrix composites reinforced with in situ devitrified Al–Ni–La amorphous particles. Scr Mater 54(5):869–874
15. Sankaranarayanan S, Shankar VH, Jayalakshmi S, Bau NQ, Gupta M (2015) Development of high performance magnesium composites using $Ni_{50}Ti_{50}$ metallic glass reinforcement and microwave sintering approach. J Alloy Compd 627:192–199
16. Tun KS, Gupta M (2007) Improving mechanical properties of magnesium using nano-yttria reinforcement and microwave assisted powder metallurgy method. Compos Sci Technol 67(13):2657–2664
17. Paramsothy M, Hassan SF, Srikanth N, Gupta M (2009) Enhancing tensile/compressive response of magnesium alloy AZ31 by integrating with Al_2O_3 nanoparticles. Mater Sci Eng A 527(1–2):162–168
18. Hassan SF, Gupta M (2004) Development of high performance magnesium nanocomposites using solidification processing route. Mater Sci Technol 20(11):1383–1388
19. Hassan SF, Gupta M (2005) Development of high performance magnesium nano-composites using nano-Al_2O_3 as reinforcement. Mater Sci Eng A 392(1–2):163–168
20. Hassan SF, Gupta M (2006) Effect of different types of nano-size oxide particulates on microstructural and mechanical properties of elemental Mg. J Mater Sci 41(8):2229–2236
21. Wong WLE, Karthik S, Gupta M (2005) Development of hybrid Mg/Al_2O_3 composites with improved properties using microwave assisted rapid sintering route. J Mater Sci 40(13):3395–3402
22. Hou J, Zhao N, Zhu S (2011) Influence of cutting speed on flank temperature during face milling of magnesium alloy. Mater Manuf Process 26(8):1059–1063
23. Rubio EM, Villeta M, Carou D, Saá A (2014) Comparative analysis of sustainable cooling systems in intermittent turning of magnesium pieces. Int J Precis Eng Manuf 15(5):929–940
24. Villeta M, de Agustina B, de Pipaón JMS, Rubio EM (2012) Efficient optimisation of machining processes based on technical specifications for surface roughness: application to magnesium pieces in the aerospace industry. Int J Adv Manuf Technol 60(9–12):1237–1246
25. Fang FZ, Lee LC, Liu XD (2005) Mean flank temperature measurement in high speed dry cutting of magnesium alloy. J Mater Process Technol 167(1):119–123
26. Singh S (2016) Study the drilling behaviour of aluminium 6061 metal matrix composites using Taguchi's methodology. Int J Mach Mach Mater 18(4):327–340
27. Mohan B, Rajadurai A, Satyanarayana KG (2004) Electric discharge machining of Al–SiC metal matrix composites using rotary tube electrode. J Mater Process Technol 153:978–985
28. Gok A (2015) A new approach to minimization of the surface roughness and cutting force via fuzzy TOPSIS, multi-objective grey design and RSA. Measurement 70:100–109
29. Wang MY, Chang HY (2004) Experimental study of surface roughness in slot end milling AL2014-T6. Int J Mach Tools Manuf 44(1):51–57
30. Puertas I, Luis CJ (2004) A study of optimization of machining parameters for electrical discharge machining of boron carbide. Mater Manuf Process 19(6):1041–1070
31. Saikumar S, Shunmugam MS (2006) Parameter selection based on surface finish in high-speed end-milling using differential evolution. Mater Manuf Process 21(4):341–347
32. Kıvak T (2014) Optimization of surface roughness and flank wear using the Taguchi method in milling of Hadfield steel with PVD and CVD coated inserts. Measurement 50:19–28
33. Rubio EM, Valencia JL, Saá AJ, Carou D (2013) Experimental study of the dry facing of magnesium pieces based on the surface roughness. Int J Precis Eng Manuf 14(6):995–1001
34. Villeta M, Rubio EM, De Pipaón JS, Sebastián MA (2011) Surface finish optimization of magnesium pieces obtained by dry turning based on Taguchi techniques and statistical tests. Mater Manuf Process 26(12):1503–1510
35. De Pipaon JS, Rubio E, Villeta M, Sebastian M (2008) Influence of cutting conditions and tool coatings on the surface finish of workpieces of magnesium obtained by dry turning. In: Annals of DAAAM & proceedings, pp 1207–1209

36. Sáenz De Pipaón JM, Rubio EM, Viletta M, Sebastián MA (2009) Improved model for estimating the expected roughness in dry turning of magnesium UNS M11311. In: Annals of DAAAM for 2009 & proceedings of the 20th international DAAAM symposium" intelligent manufacturing & automation: focus on theory, practice and education, vol 20, No 1, pp 319–320)
37. Wang Q, Liu F, Wang X (2014) Multi-objective optimization of machining parameters considering energy consumption. Int J Adv Manuf Technol 71(5–8):1133–1142
38. Viswanathan R, Ramesh S, Subburam V (2018) Measurement and optimization of performance characteristics in turning of Mg alloy under dry and MQL conditions. Measurement 120:107–113
39. Davim JP, Sreejith PS, Silva J (2007) Turning of brasses using minimum quantity of lubricant (MQL) and flooded lubricant conditions. Mater Manuf Process 22(1):45–50
40. Zhang S, Li JF, Wang YW (2012) Tool life and cutting forces in end milling Inconel 718 under dry and minimum quantity cooling lubrication cutting conditions. J Clean Prod 32:81–87
41. Attanasio A, Gelfi M, Giardini C, Remino C (2006) Minimal quantity lubrication in turning: effect on tool wear. Wear 260(3):333–338
42. Carou D, Rubio EM, Lauro CH, Davim JP (2016) The effect of minimum quantity lubrication in the intermittent turning of magnesium based on vibration signals. Measurement 94:338–343
43. Carou D, Rubio EM, Davim JP (2015) A note on the use of the minimum quantity lubrication (MQL) system in turning. Ind Lubr Tribol 67(3):256–261
44. Davim JP, Sreejith PS, Gomes R, Peixoto C (2006) Experimental studies on drilling of aluminium (AA1050) under dry, minimum quantity of lubricant, and flood-lubricated conditions. Proc Inst Mech Eng Part B J Eng Manuf 220(10):1605–1611
45. Gaitonde VN, Karnik SR, Davim JP (2012) Optimal MQL and cutting conditions determination for desired surface roughness in turning of brass using genetic algorithms. Mach Sci Technol 16(2):304–320
46. Gupta K, Laubscher RF, Davim JP, Jain NK (2016) Recent developments in sustainable manufacturing of gears: a review. J Clean Prod 112:3320–3330
47. Deng JL (1989) Introduction to Grey system theory. J Grey Syst 1(1):1–24
48. Opricovic S, Tzeng GH (2004) Compromise solution by MCDM methods: a comparative analysis of VIKOR and TOPSIS. Eur J Oper Res 156(2):445–455
49. Buldum B, Eşme U, Kemal Külekci M, Şik A, Kazançoğlu Y (2012) Use of Grey-Taguchi method for the optimization of oblique turning process of AZ91D magnesium alloy. Mater Test 54(11–12):779–785
50. Gopal PM, Prakash KS (2018) Minimization of cutting force, temperature and surface roughness through GRA, TOPSIS and Taguchi techniques in end milling of Mg hybrid MMC. Measurement 116:178–192
51. Lalwani DI, Mehta NK, Jain PK (2008) Experimental investigations of cutting parameters influence on cutting forces and surface roughness in finish hard turning of MDN250 steel. J Mater Process Technol 206(1–3):167–179
52. Pawade RS, Sonawane HA, Joshi SS (2009) An analytical model to predict specific shear energy in high-speed turning of Inconel 718. Int J Mach Tools Manuf 49(12–13):979–990
53. Motorcu AR, Isik Y, Kus A, Cakir MC (2016) Analysis of the cutting temperature and surface roughness during the orthogonal machining of AISI 4140 alloy steel via the Taguchi method. Analysis 343:351
54. Suneesh E, Sivapragash M (2017) Mechanical performance of magnesium composites containing hybrid Al_2O_3 reinforcement. Int J Civ Eng Technol (IJCIET) 8(8):365–378
55. El-Hofy HAG (2013) Fundamentals of machining processes: conventional and nonconventional processes. CRC Press, Boca Raton
56. Mia M, Dhar NR (2017) Optimization of surface roughness and cutting temperature in high-pressure coolant-assisted hard turning using Taguchi method. Int J Adv Manuf Technol 88(1–4):739–753
57. Mia M, Rifat A, Tanvir MF, Gupta MK, Hossain MJ, Goswami A (2018) Multi-objective optimization of chip-tool interaction parameters using Grey-Taguchi method in MQL-assisted turning. Measurement 129:156–166
58. Mia M, Al Bashir M, Khan MA, Dhar NR (2017) Optimization of MQL flow rate for minimum cutting force and surface roughness in end milling of hardened steel (HRC 40). Int J Adv Manuf Technol 89(1–4):675–690
59. Srinivasan L, Chand KM, Kannan TDB, Sathiya P, Biju S (2018) Application of GRA and TOPSIS optimization techniques in GTA welding of 15CDV6 aerospace material. Trans Indian Inst Met 71(2):373–382
60. Kilickap E, Yardimeden A, Çelik YH (2017) Mathematical modelling and optimization of cutting force, tool wear and surface roughness by using artificial neural network and response surface methodology in milling of Ti-6242S. Appl Sci 7(10):1064
61. Çiçek A, Kıvak T, Ekici E (2015) Optimization of drilling parameters using Taguchi technique and response surface methodology (RSM) in drilling of AISI 304 steel with cryogenically treated HSS drills. J Intell Manuf 26(2):295–305
62. Eker B, Ekici B, Kurt M, Bakır B (2014) Sustainable machining of the magnesium alloy materials in the CNC lathe machine and optimization of the cutting conditions. Mechanics 20(3):310–316
63. Williams JA, Tabor D (1977) The role of lubricants in machining. Wear 43(3):275–292
64. Hong SY, Ding Y (2001) Cooling approaches and cutting temperatures in cryogenic machining of Ti-6Al-4V. Int J Mach Tools Manuf 41(10):1417–1437
65. Gupta MK, Sood PK, Singh G, Sharma VS (2017) Experimental investigation and optimization on MQL-assisted turning of Inconel-718 super alloy. In: Advanced manufacturing technologies, pp 237–248. Springer, Cham
66. Stephenson DA, Agapiou JS (2016) Metal cutting theory and practice. CRC Press, Boca Raton
67. Sivasakthivel PS, Sudhakaran R (2013) Optimization of machining parameters on temperature rise in end milling of Al 6063 using response surface methodology and genetic algorithm. Int J Adv Manuf Technol 67(9–12):2313–2323
68. Wojciechowski S, Maruda RW, Krolczyk GM, Niesłony P (2018) Application of signal to noise ratio and grey relational analysis to minimize forces and vibrations during precise ball end milling. Precis Eng 51:582–596